



Article

Effect of Alkali Metal Atoms Doping on Structural and Nonlinear Optical Properties of the Gold-Germanium Bimetallic Clusters

Xiaojun Li *, Shuna Li, Hongjiang Ren, Juxiang Yang and Yongqiang Tang

The Key Laboratory for Surface Engineering and Remanufacturing in Shaanxi Province, School of Chemical Engineering, Xi'an University, Xi'an 710065, China; lishuna101@163.com (S.L.); hjren@xawl.edu.cn (H.R.); juxiangyang03@126.com (J.Y.); yqtang11@163.com (Y.T.)

* Correspondence: xjli@xawl.edu.cn; Tel.: +86-029-8827-9060

Received: 16 June 2017; Accepted: 10 July 2017; Published: 17 July 2017

Abstract: A new series of alkali-based complexes, AM@Ge_nAu (AM = Li, Na, and K), have been theoretically designed and investigated by means of the density functional theory calculations. The geometric structures and electronic properties of the species are systematically analyzed. The adsorption of alkali metals maintains the structural framework of the gold-germanium bimetallic clusters, and the alkali metals prefer energetically to be attached on clusters' surfaces or edges. The high chemical stability of Li@Ge₁₂Au is revealed by the spherical aromaticity, the hybridization between the Ge atoms and Au-4d states, and delocalized multi-center bonds, as well as large binding energies. The static first hyperpolarizability (β_{tot}) is related to the cluster size and geometric structure, and the AM@Ge_nAu (AM = Na and K) clusters exhibit the much larger β_{tot} values up to 13050 a.u., which are considerable to establish their strong nonlinear optical (NLO) behaviors. We hope that this study will promote further application of alkali metals-adsorbed germanium-based semiconductor materials, serving for the design of remarkable and tunable NLO materials.

Keywords: semiconductor clusters; electronic structures; chemical bondings; spherical aromaticity; NLO properties

1. Introduction

Alkali metals have attracted much attention because they serve as building blocks for novel materials with tunable properties [1], and a great deal of new alkali-based complexes have been recently reported [2–4]. In particular, a series of alkalides, proposed as the candidates of nonlinear optical (NLO) materials, exhibit exceptionally large NLO responses and are promising for their spectacular semiconductor potentials in photoelectricity devices and optical communications, e.g., M@C₆₀ (M = Li, Na, Cs) [5], Li@C₆₀-BX₄ (X = F, Cl, Br) [6], Li_nF ($n = 2-5$) [7], Li₂@BN nanotubes [8], OLi₃-M-Li₃O (M = Li, Na, K) [9], Li₃⁺(calyx[4]pyrrole)M⁻ [10], Li(NH₃)₄M (M = Li, Na, K) [11], and Li(CH₃NH₂)_nNa [12], etc., in which both theoretical and experimental studies play a crucial role in finding ways to enhance the NLO behaviors. On the other hand, the different NLO materials can be expressed by the largely high second-order NLO response at the molecular level [13,14], and the first hyperpolarizability can be quantitatively used to evaluate the potential NLO materials of alkali-based complexes.

Meanwhile, owing to the unique electronic properties of alkalides, their derivatives have been extensively reported with the extension to silicon-based clusters, e.g., Si₁₀(Li, Na, K)_n ($n = 1, 2$) [15], (Li, Na, K)@Si_nNb ($n = 1-12$) [16], Si₁₀Li₈ [17], and Si_nFe ($n = 1-14$) [18], which ascribe to loosely bound electrons in alkali-based complexes, resulting in the large NLO responses. It is also noteworthy that although the analogous germanium and silicon species are isovalent, their structures and

physicochemical properties are quite different [19–25]. For example, the static hyperpolarizabilities of pure Si_mGe_n ($m + n = 7$, $n = 0–7$) clusters were studied by using the density functional theory (DFT) and MP2 ab initio methods [26], and revealed that the enhancement of the hyperpolarizabilities arises from more polarizable character on the germanium atoms, and thus alkali metals-adsorbed germanium-based semiconductor clusters may have the unusual features in high-performance optoelectronic devices for the potential applications. In addition, Knoppe and Ozga et al. [27–29] found that the gold-containing clusters appear to have strong NLO responses, and the Au atom plays an important role in the optoelectronic application. Obviously, the knowledge of geometries, electronic structures, chemical bonding, and nonlinear optical properties of the species is very important for understanding these applications, but these are rarely reported. With this motivation, we explored the stability and electronic structures of alkali metals-adsorbed Ge_nAu semiconductor clusters for the first time, labeled as $\text{AM@Ge}_n\text{Au}$ ($\text{AM} = \text{Li, Na, and K}$; $n = 2–13$), and investigated the effect of alkali metals on the dipole moment, polarizability, and first hyperpolarizability (β_{tot}). The results suggest that the $\text{AM@Ge}_n\text{Au}$ ($\text{AM} = \text{Na and K}$) clusters may be proposed as novel potential high-performance NLO materials, especially for the $\text{Na@Ge}_7\text{Au}$ cluster with a large β_{tot} value.

2. Computational Details

The geometrical optimizations of the $\text{AM@Ge}_n\text{Au}$ ($\text{AM} = \text{Li, Na, and K}$; $n = 2–13$) clusters were carried out by using the hybrid DFT-B3LYP functional [30,31], implemented in the Gaussian 09 suite of programs [32]. This method provides a good prediction on energy evaluation [33–35], in conjunction with the Karlsruhe split-valence basis set augmented with polarization functions (def-SVP) for all alkali metal atoms and the double- ζ LanL2DZ [36–38] with effective core potentials (ECPs) for the Ge and Au atoms, and then the low-lying isomers are further reoptimized at the B3LYP/def-TZVP level of theory. In the calculations, the singlet and triplet spin states were examined for each initial structure, and the zero-point vibrational correction was included into the relative energies. According to the previous works on the neutral [24] and cationic [39] Ge_nAu clusters, we searched a large number of initial isomers for the alkali metals-adsorbed gold-doped germanium clusters from the following steps. One is that the alkali metal atoms are attached to different germanium positions on the surface, edge or apex of the lowest-energy structures of the Ge_nAu clusters. The second is the attaching structure with gold positions adsorbed by alkali metals. The remaining structures were constructed by us. Vibrational frequency computations were conducted to ensure that these low-lying structures are local minima on its potential energy surface.

The energy of a molecular system in the presence of a homogeneous electric field can be written as the following equation [40–42]:

$$E(F) = E^0 - \mu_i F_i - \frac{1}{2} \alpha_{ij} F_i F_j - \frac{1}{6} \beta_{ijk} F_i F_j F_k - \frac{1}{24} \gamma_{ijkl} F_i F_j F_k F_l \cdots \quad (1)$$

Here, E^0 is the total energy of the molecule without electric field present, F_i is the electric field component in the i direction; the μ_i , α_{ij} , β_{ijk} terms are the dipole, the polarizability, and the first hyperpolarizability, respectively. The static dipole moment (μ_0) and polarizability (α_{iso}) are defined as follows:

$$\mu_0 = (\mu_x^2 + \mu_y^2 + \mu_z^2)^{1/2} \quad (2)$$

$$\alpha_{\text{iso}} = (\alpha_{xx} + \alpha_{yy} + \alpha_{zz})/3 \quad (3)$$

The static first hyperpolarizability (β_{tot}) is obtained as follows:

$$\beta_{\text{tot}} = (\beta_x^2 + \beta_y^2 + \beta_z^2)^{1/2} \quad (4)$$

where $\beta_i = (1/3) \sum_j (\beta_{ijj} + \beta_{jji} + \beta_{jij})$, $i, j = \{x, y, z\}$.

The density-of-states (DOS) spectra were convoluted utilizing the GaussSum 2.2 program [43] with the full-width at half maximum (FWHM) of 0.3 eV. Chemical bonding analyses were performed using the adaptive natural density partitioning (AdNDP) method proposed by Zubarev and Boldyrev [44]. The molecular orbitals were plotted with the isodensity surfaces ($0.02 e^{1/2}/(\text{bohr})^{3/2}$), and the molecular graphs were visualized using the VMD program [45]. The long-range corrected functional CAM-B3LYP [46] was utilized to calculate the excited energies within the framework of the time-dependent density functional theory (TDDFT) [47], as well as for the evaluation of linear and nonlinear (L&NLO) optical properties, e.g., dipole moments (μ_0), isotropic polarizability (α_{iso}), and first hyperpolarizability (β_{tot}) of the $\text{AM@Ge}_n\text{Au}$ clusters.

3. Results and Discussion

3.1. Geometric Structures

The low-lying structures of the $\text{AM@Ge}_n\text{Au}$ ($n = 2\text{--}13$) clusters are displayed in Figure 1. The relative energies of these low-lying isomers, obtained by using the two basis sets as mentioned above, are listed in Table S1 of Supplementary Materials, in which all the calculations indicate that the global minimum for each cluster is in singlet spin states. Meanwhile, one can see from Figure 1 that adsorption of the AM atoms does not largely change the structural framework of the Au-doped germanium clusters, as reported previously by Li et al. [24], and the alkali metals prefer to be attached on clusters' surface or edge with the multi-adsorbed bonds (multi-bonds) rather than the AM–Ge or AM–Au single-adsorbed bond in the stable structures.

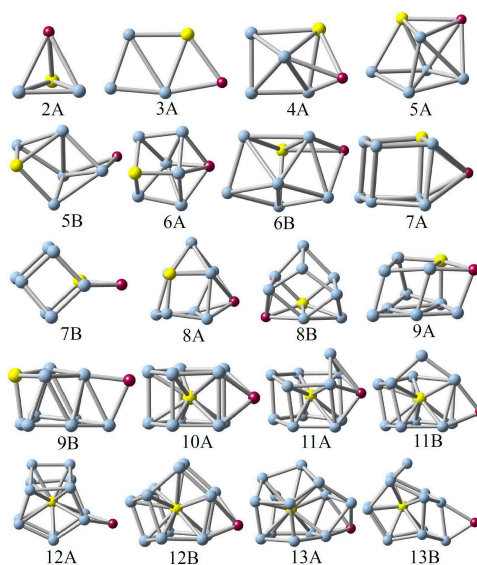


Figure 1. Low-lying structures of the $\text{AM@Ge}_n\text{Au}$ ($n = 2\text{--}13$) clusters, obtained by using the hybrid B3LYP functional. The blue, yellow and purple balls represent the Ge, Au and alkali metal (AM) atoms, respectively.

(Li, Na, K)@Ge₂Au. The lowest-energy structure (2A) of $\text{AM@Ge}_2\text{Au}$ (AM = Li, Na, and K) takes the tetrahedron structure with C_s symmetry, generated from the AM atoms being capped on the clusters' surface of the triangular Ge–Ge–Au base. The corresponding triplet states are less stable in energy than those with singlet spin states by 1.03–1.43 eV high at the B3LYP/def-TZVP level of theory (see Table S1 of Supplementary Materials). According to our calculations, the equilibrium Ge–Ge bond lengths are predicted to be 2.399–2.601 Å in the $\text{AM@Ge}_2\text{Au}$ clusters.

(Li, Na, K)@Ge₃Au. 3A is a planar structure with C_s symmetry, which can be regarded as the alkali metals being bonded on the edge (Au–Ge) of the rhombic Ge_3Au cluster, whereas the structure

adsorbed on another edge (Ge–Ge) by alkali metals can be found to be unstable. The 3A geometry can be considered as the global minimum of the AM@Ge₃Au (AM = Li, Na, and K) cluster. In Li@Ge₃Au, the equilibrium bond lengths are evaluated to be 2.597 Å for the Li–Au bond, 2.515 Å for the Li–Ge bond, 2.558–2.722 Å for two Au–Ge bonds, and 2.353–2.876 Å for three Ge–Ge bonds.

(Li, Na, K)@Ge₄Au. As previously reported [24], the ground-state structure of the Ge₄Au cluster is a pyramid-distorted isomer. When the AM atoms are attached on the side face (Ge–Ge–Au) of Ge₄Au, the most stable 4A structure is formed, in which the equilibrium Li–Ge and Li–Au bond lengths are predicted to be 2.597, 2.615, and 2.771 Å at the B3LYP/def-TZVP level of theory, respectively.

(Li, Na, K)@Ge₅Au. In the search for the low-lying configurations of AM@Ge₅Au (AM = Li, Na, and K), there are two stable structures (5A and 5B) with close energies (0.13–0.16 eV in singlet spin states) to be obtained while their triplet spin states have the higher relative energies (at least 0.78 eV) at the B3LYP/def-TZVP level of theory. The geometric differences between the two isomers are that the AM atoms are adsorbed on the side face (Ge–Ge–Ge–Au) or side edge (Ge–Ge) of the distorted triangular prism. Obviously, the global minimum of AM@Ge₅Au (AM = Li, Na, and K) is found to be the 5A structure. It is noteworthy that for small clusters with $n \leq 5$, the lowest-energy structures take the AM-adsorbed on Au-adjacent edge or surface of cluster base, to form the stable AM–Au chemical bonds.

(Li, Na, K)@Ge₆Au. Similar to the $n = 5$ cluster as discussed above, we have manually designed a great number of initial geometries for the $n = 6$ cluster size, e.g., adsorbing the AM atoms to different position sites and substituting the apical Ge atom by the AM atoms in the Ge₇Au cluster, and so on, but the 6A cage-like with C_s symmetry is the lowest-energy structure for the AM@Ge₆Au (AM = Li, Na, and K). The 6B isomer is a distorted quadrangular prism, which is less stable than 6A by at least 0.13 eV higher in energy. Meanwhile, it is found that the two different basis sets used herein provide the same energetic ordering for these small clusters (see Table S1 of Supplementary Materials).

(Li, Na, K)@Ge₇Au. As mentioned above, the AM atoms prefer energetically to be adsorbed on the Au-adjacent surface (Ge–Ge–Ge–Au) or edge (Ge–Au) of the quadrangular prism (QP), thus the two stable structures (7A and 7B) can be obtained. According to our calculation, the 7A isomer is predicted as a putative global minimum for the (Li, K)@Ge₇Au clusters, whereas the 7B isomer is the most stable structure for Na@Ge₇Au.

(Li, Na, K)@Ge₈Au. The 8A and 8B isomers are one bicapped square prism, which can be viewed as the alkali metal and Au atom capped on different faces of the lowest-energy Ge₇Au cluster (called as square prism). Of which 8A is the lowest-energy structure for the Li@Ge₈Au cluster at the B3LYP/LanL2DZ(Ge,Au)/def-SVP(AM) level of theory, while the most stable structure for (Na, K)@Ge₈Au is the 8B isomer lying only 0.02–0.04 eV under the 8A isomer. However, the energetic ordering of 8A and 8B for (Na, K)@Ge₈Au can be reversed at the B3LYP/Def-TZVP level of theory. Thus, the 8A geometry can be found to be the global minimum for the AM@Ge₈Au (AM = Li, Na, and K) cluster at the B3LYP/Def-TZVP level of theory.

(Li, Na, K)@Ge₉Au. Based on the lowest-energy Ge₉Au cluster [24], the alkali metal-adsorbed complexes can be generated from the AM atoms attaching on the above Au–Ge layer. It is obvious that the Au-adjacent isomer (9A) is more stable than the Au-outlying one (9B) by ~0.04–0.06 eV in singlet spin states, being consistent with the small clusters ($n \leq 5$).

(Li, Na, K)@Ge₁₀Au. The Ge₁₀Au cluster is a C_{2v}-symmetrical pentagonal prism with the Au-encapsulated into the central position of structure [24]. When the alkali metal atoms are directly face-capped on side quadrangle of Ge₁₀Au, a new equilibrium 10A structure, considered as global minimum, is yielded using the DFT-B3LYP functional. Of which the theoretical bond lengths are predicted to be 2.769 Å for the four equivalent Li–Ge bonds, and 2.715, 2.733, and 2.742 Å for three kinds of the equivalent Ge–Au bonds.

(Li, Na, K)@Ge₁₁Au. The 11A structure can be regarded as the Ge atom being directly capped on the side edge of the above pentagon of 10A or alkali metal atoms being directly adsorbed on the face-sided pentagon of the lowest-energy Ge₁₁Au cluster, as published previously [24]. Similarly, the

low-lying 11B isomer can be formed by capping the alkali metal atoms on the face-sided quadrangle of the Ge₁₁Au cluster, which is less stable than 11A by at least 0.07 eV high in energy (see Table S1 of Supplementary Materials).

(Li, Na, K)@Ge₁₂Au. Similar to the $n = 11$ cluster as discussed above, the 12A and 12B structures can be generated from the different position sites adsorbed by alkali metal atoms on the lowest-energy Ge₁₂Au cluster. Interestingly, the 12B isomer has a highly coordinated surface adsorbed by the Li atom to eliminate the number of dangling bonds on the clusters' surface, regarded as the global minimum of Li@Ge₁₂Au. Contrastingly, the adsorption of Na/K in lower coordinated edge position (12A) will form the lowest-energy structure for (Na, K)@Ge₁₂Au cluster.

(Li, Na, K)@Ge₁₃Au. Referring to the equilibrium geometries of the low-lying Ge₁₃Au cluster reported previously [24], a great number of initial structures of alkali metal-adsorbed complexes were extensively constructed and optimized in order to locate the global minimum of the cluster size. For comparison, we only show two first stable 13A and 13B isomers for (Li, Na, K)@Ge₁₃Au (see Figure 1), which shows the close energy difference between 0.03 eV and 0.22 eV at the B3LYP/Def-TZVP level of theory (see Table S1 of Supplementary Materials). Obviously, the lowest-energy 13A structure undergoes the structural relaxation, whereas the low-lying 13B structure keeps the structural framework of the lowest-energy Ge₁₃Au cluster.

3.2. Chemical Stability and Electronic Structures

In order to explore the size selectivity and the electronic properties of the AM@Ge_{*n*}Au ($n = 2-13$) clusters, we plotted the average binding energy (E_b), the dissociation energy (D_e , AM@Ge_{*n*}Au → Ge_{*n*}Au + AM), the HOMO-LUMO gaps (GAPs), and the vertical ionization potentials (VIP) and vertical electron affinities (VEA) in Figures 2 and 3, respectively, which are defined by:

$$E_b(n) = [E(\text{AM}) + nE(\text{Ge}) + E(\text{Au}) - E(\text{AM@Ge}_n\text{Au})]/(n + 2) \quad (5)$$

$$D_e(n) = E(\text{Ge}_n\text{Au}) + E(\text{AM}) - E(\text{AM@Ge}_n\text{Au}) \quad (6)$$

where the E term represents the total energy with zero-point vibrational corrections.

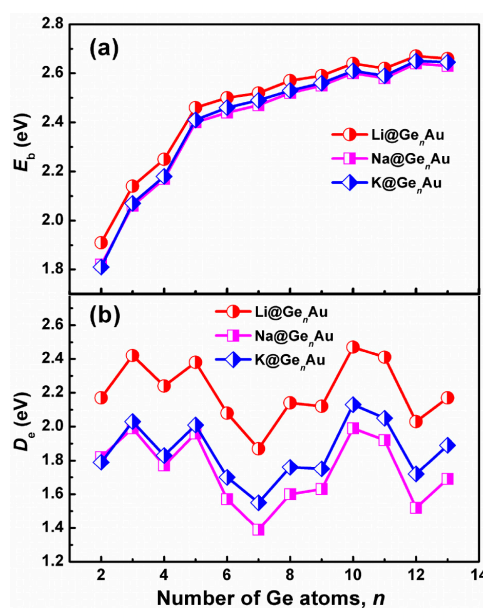


Figure 2. Size dependences of (a) the average binding energies (E_b) and (b) dissociation energies (D_e) for the AM@Ge_{*n*}Au ($n = 2-13$) clusters, obtained by using the hybrid B3LYP functional, in conjunction with the Def-TZVP basis set.

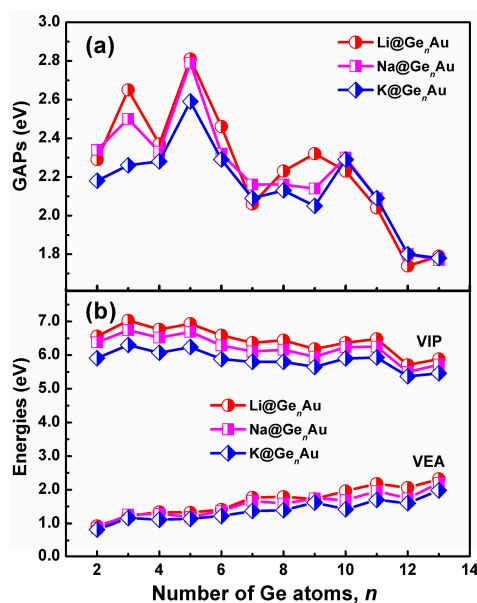


Figure 3. Size dependences of (a) HOMO-LUMO gaps (GAPs), and (b) vertical ionization potentials (VIP) and vertical electron affinities (VEA) for the $AM@Ge_nAu$ ($n = 2-13$) clusters, obtained by using the hybrid B3LYP functional, in conjunction with the Def-TZVP basis set.

It is well known that a larger E_b value indicates a higher chemical stability of cluster. We can see from Figure 2a that the average binding energies of $AM@Ge_nAu$ ($AM = Na$ and K) have almost similar values for each cluster size, which are slightly lower than that of $Li@Ge_nAu$ by $\sim 0.03-0.10$ eV. However, all of the $AM@Ge_nAu$ ($AM = Li, Na,$ and K) clusters show the same increased trends. For example, their average binding energies dramatically increase up to the size of $n = 5$ and smoothly increase with the size $n = 6-13$, indicating that the large-sized doped clusters are more stable than the small-sized ones, especially for the $n = 10$ and 12 clusters. The dissociation energy (D_e) with the removal of the AM atoms is another useful physical quantity that can also reflect the relative stability of $AM@Ge_nAu$. It is apparent from Figure 2b that the $n = 3, 5,$ and 10 clusters are the local maximum D_e peaks, which are more stable than their corresponding neighbors. Meanwhile, the D_e energetic ordering by alkali metals is $Li > K > Na$.

The HOMO-LUMO gaps (GAPs) of the $AM@Ge_nAu$ clusters are listed in Figure 3a. One can find that the gaps (2.04–2.81 eV) in the small-sized clusters with the size $n \leq 11$ are larger than those, 1.74–1.80 eV, in the large-sized clusters. Clearly, the HOMO-LUMO gap values with $n = 12$ and 13 lie in the typically optical region (e.g., less than 2 eV), making these clusters attractive for the cluster-assembled optoelectronic materials, which are consistent with previous reports[48], e.g., $Zn@Ge_{12}$ and $Cd@Sn_{12}$.

The vertical ionization potentials (VIPs) and vertical electron affinities (VEAs) of $AM@Ge_nAu$ ($n = 2-13$) are considered to explore the dependence of electronic structures on the cluster size. The VIP can be evaluated by the energy difference between the optimized neutral species and single-point cationic species at the optimized neutral geometry. The VEA can be computed by adding one electron to the neutral species in its equilibrium geometry and taking their energy differences. The calculated VIPs and VEAs of the most stable clusters are plotted in Figure 3b. As shown in Figure 3b, the curve reveals that there is a gradually decreased behavior for VIPs along with increasing number of Ge atom, and the cluster with small VIPs (e.g., $n = 12$) will be more close to a metallic species [49]; reversely, there is a gradually increased trend for VEAs. Similar to the E_b and D_e values, the $Li@Ge_nAu$ clusters give the larger VIPs and VEAs than the Na- and K-based complexes. It is notable that the VIPs of $AM@Ge_{10}Au$ ($AM = Na$ and K) are 5.48 eV and 5.32 eV, respectively, smaller than that of Li (5.62 eV)

and Na (5.40 eV), respectively, indicating these clusters should have an electronic structure reminiscent of an alkali atom.

3.3. Density of States

To further investigate the electronic effect of the alkali metals adsorption on the clusters' surface, we explored the total (TDOS) and partial (PDOS) density of states, taking the stable Li@Ge₁₂Au (12B) cluster as a typical case, shown in Figure 4, which includes all atomic contributions (Li, Ge, and Au) of the clusters to PDOS, while the contributions of different atomic shells (*s*, *p*, *d*) to the molecular orbitals (MOs) are also discussed.

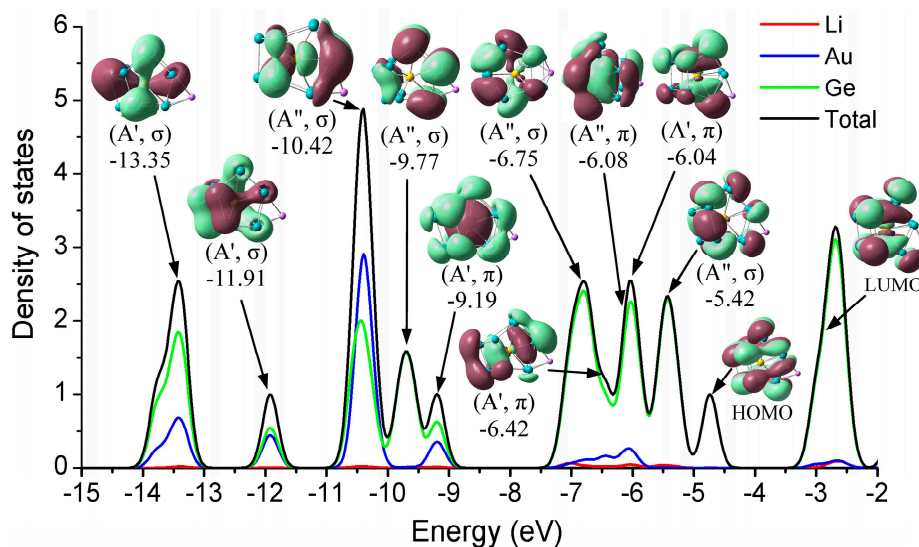


Figure 4. Total (DOS) and partial (PDOS) density of states of the most stable Li@Ge₁₂Au (12B) cluster, and the valence orbitals are obtained at the B3LYP/def-TZVP level of theory. The atomic contributions (Li, Au, and Ge) of the cluster to the DOS spectrum are labeled.

As for this case, each Ge atom is expected to contribute its four valence electrons ($4s^2 4p^2$) to the shell configuration while the Li and Au atoms can contribute one ($2s^1$) and eleven ($5d^{10} 6s^1$) valence electrons, respectively. Thus, the Li@Ge₁₂Au cluster with C_s symmetry contains 60 valence electrons, which are distributed in the following orbital configuration: $(1a')^2(2a')^2(1a'')^2(3a')^2(2a'')^2(3a'')^2(4a')^2(5a')^2(6a')^2(4a'')^2(5a'')^2(7a')^2(8a')^2(6a'')^2(9a')^2(7a'')^2(10a')^2(11a')^2(12a')^2(13a')^2(8a'')^2(14a')^2(15a')^2(9a'')^2(16a')^2(10a'')^2(17a')^2(11a'')^2(18a')^2(12a'')^2$. The main valence molecular orbitals ($0.02 e/a.u.^3$) of the cluster are depicted in Figure 4. We can clearly see that, for the stable Li@Ge₁₂Au (12B) clusters, the σ -type HOMO has an interesting double pumpkin shape with the electron cloud delocalized on the two sides of the Ge–Ge–Au cross section, mostly involving the five-membered Ge₅ rings, due to the hybridization of 12.38% Ge-4s and 85.51% Ge-4p states, whereas the σ -type LUMO originates mainly from the dominant interactions between Au-5d_{xz} state and 4s4p hybridized orbitals of the Ge₁₂ cage. The Au-5d_{xz} orbital has only 3.37% contribution to the LUMO, while the 4s4p hybridized orbitals of 12 Ge atoms have 93.70% contribution to the LUMO. Obviously, the small HOMO-LUMO gap (1.74 eV) of the cluster should be largely related to the electron distributions of the frontier molecular orbitals, and the hybridization of Ge atoms with metal dopants can increase the HOMO-LUMO gap, and enhance the chemical stability of the cluster [22]. The strongest DOS band at around -10.42 eV mainly ascribes to the σ -type HOMO-19 orbital, which comes mostly from different atomic shells, e.g., 66.77% Au-*d*_{yz}, 23.19% Ge-4s, and 2.92% Ge-4p_y states. In addition, the Au-4d states have strong interactions (28.86%, 46.57%, and 14.26%) with Ge atoms for HOMO-22 (-13.35 eV), HOMO-21 (-11.91 eV), and HOMO-12 (-9.19 eV) orbitals, respectively, indicating that the 4d states of Au atom in these orbitals are involved in the chemical bonding. One can see that the

valence electron orbitals of $\text{Li@Ge}_{12}\text{Au}$ are divided into two different subsets occupied by σ and π electrons, and the doped cluster contains eight valence π -electrons in four molecular orbitals, e.g., $-9.19(A', \pi)$, $-6.42(A', \pi)$, $-6.08(A'', \pi)$, and $-6.04(A', \pi)$ orbitals, which belong to one 1S- and three 1P-subshells of the doped cluster, according to the electron shell model [22,50,51].

3.4. Chemical Bonding Analysis

In order to further explore the bonding properties of metal dopant and Ge atoms, we performed the adaptive natural density partitioning (AdNDP) analysis proposed by Zubarev and Boldyrev [44], taking the most stable $\text{Li@Ge}_{12}\text{Au}$ (12B) cluster as an example. The AdNDP method is based on the concept of electron pairs as the main elements of chemical bonding, and represents the electronic structure in terms of n -center two-electron (nc -2e) bonds, in which the n values go from one (lone-pair) to the maximum number of clusters. This method has been successfully applied to gain insight into the bonding characters not only for fullerene derivatives [41], but also for boron [52–55] and transition-metal doped Si/Ge clusters [22].

In the method, the occupation numbers (ONs) indicate the number of electrons per bond, and the ONs exceed the established threshold value and are close to the ideal limit of $2.00 |e|$. As mentioned above, the $\text{Li@Ge}_{12}\text{Au}$ (12B) cluster has 60 valence electrons and thus 30 chemical bonds with each bond occupied by two electrons. According to the AdNDP results, there are five typical d -lone pairs (LPs) on Au with $\text{ON} = 1.93$ – $1.98 |e|$, and eight s -lone pairs on the Ge atoms with $\text{ON} = 1.75$ – $1.78 |e|$ (see Figure 5), which reveals that electrons on the Ge atoms are not completely localized into lone pairs, but partially participate into the localized or delocalized bondings. As can be seen from Figure 5, ten two-center two-electron ($2c$ -2e) σ -bonds are localized on clusters' surface with $\text{ON} = 1.74$ – $1.91 |e|$. Meanwhile, a total of seven delocalized σ -bonds can be readily identified: two $3c$ -2e σ -bonds ($\text{ON} = 1.74 |e|$) on the Ge-Au-Ge triangles under the cage structure, two $4c$ -2e σ -bonds ($\text{ON} = 1.71 |e|$) on the top structure, two $5c$ -2e σ -bonds ($\text{ON} = 1.81 |e|$) on the tetragonal pyramid of left structure and one $6c$ -2e σ -bonds ($\text{ON} = 1.87 |e|$) on the tetragonal bipyramid of right structure with two vertices occupied by Au and Li atoms. Obviously, the localized $2c$ -2e σ -bonds are mainly located on the clusters' surface, whereas all of the delocalized σ -bonds are always involved in the endohedral Au dopant. This indicates that the delocalized Au–Ge interactions will be responsible for the structural stabilization of the lowest-energy $\text{Li@Ge}_{12}\text{Au}$ (12B) cluster.

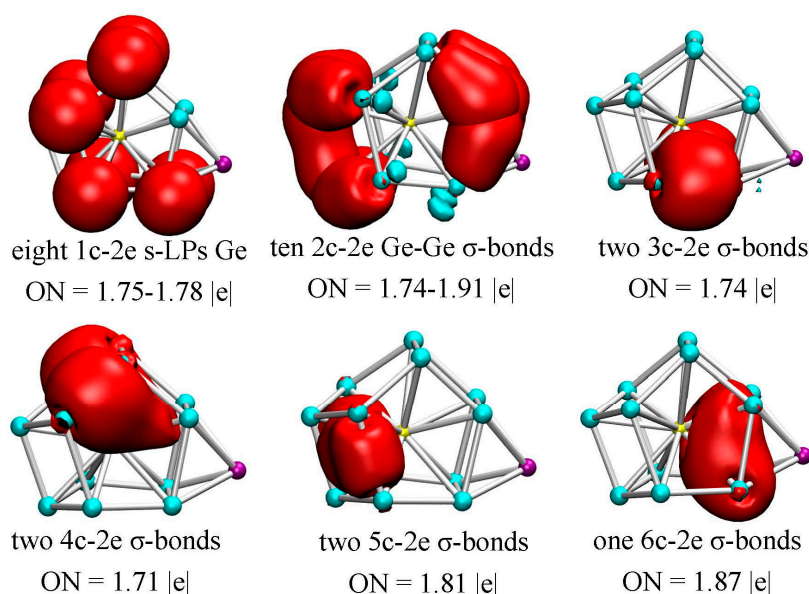


Figure 5. AdNDP chemical bonding analyses of the $\text{Li@Ge}_{12}\text{Au}$ (12B) cluster. ON denotes the electron occupation number and is close to the ideal population of $2.00 |e|$.

3.5. Spherical Aromaticity

It is well known that aromaticity is one of important measures of many compounds, and analogous aromatic compounds commonly take on high chemical stability relative to non-aromatic ones. For planar structures, the aromatic characters are identified by using the $4N + 2$ Hückel rule [56]. However, In 2000, Hirsch et al. [57] proposed another electron counting rule for three-dimensional (3D) structures, namely $2(N + 1)^2$ rule, which has been proven as an effective aromaticity criterion, with the extension to inorganic clusters [22,50,58]. In the proposal, the π -electron system of the spherical species can be approximately regarded as a spherical electron gas, which surrounds the spherical surface [59]. According to the Pauli principle, if the number of π electrons in a spherical species satisfies the $2(N + 1)^2$ counting rule, and then the 3D structures can be considered to be aromatic.

Figure 4 shows the molecular orbitals of the stable Li@Ge₁₂Au (12B) cluster. One can note that the valence electron orbitals are divided into two different orbital sets occupied by σ or π electrons. In particular, the Li@Ge₁₂Au (12B) cluster contains eight π -electrons in four molecular orbitals as mentioned above, and these π -electrons fully satisfy the $2(N_{\pi} + 1)^2 [N_{\pi} = 1]$ counting rule. As a result, the π -electron species makes Li@Ge₁₂Au spherically aromatic, and the aromatic character can be regarded as one of the main reasons in the structural stabilization of endohedrally cluster. However, the $2(N + 1)^2$ electron counting rule cannot be solely applied to explore the aromaticity of compounds, e.g., the bianionic Si₁₂²⁻ cluster contains eight π -electrons, but is predicted to be antiaromatic [60]. Therefore, the aromaticity of the Li@Ge₁₂Au (12B) cluster has to be further confirmed by the nucleus-independent chemical shifts (NICS) calculations proposed by Chen and co-workers [61], on the basis of magnetic shieldings with GIAO approximation. Aromaticity is expected to be estimated by a negative NICS value, whereas antiaromaticity is expected to be estimated by a positive NICS value. In the study, a ghost atom is placed at the center of spherical geometry to compute the NICS value. At the B3LYP/def-TZVP level of theory, it is found that the NICS(0) value is -295.7 ppm for the Li@Ge₁₂Au (12B) cluster. Thus, the aromatic character of the cluster, identified by the $2(N_{\pi} + 1)^2 [N_{\pi} = 1]$ counting rule, can be confirmed by the largely negative NICS values, and the large diatropic NICS(0) value can contribute to the high chemical stability of the geometry.

3.6. Linear and Nonlinear Optical Properties

In order to explore the L&NLO behavior of the alkali metals-adsorbed gold-doped germanium clusters, we have computed the static dipole moments (μ_0), isotropic polarizabilities (α_{iso}), and static first hyperpolarizability (β_{tot}) using the long-range corrected CAM-B3LYP functional in conjunction with the def2-TZVPD basis sets, shown in Figure 6. According to the results, it shown in Figure 6 that the doping of alkali metals (Li, Na and K) on the clusters' surface largely enhances the electric properties of the considered systems.

It is evident that the dipole moments of AM@Ge_nAu take on the fluctuating behaviors with the increasing number of Ge atom, and the local maximum peaks are found at $n = 3, 7,$ and 9 for the alkali-based complexes, which are much larger than those of bare Ge_nAu clusters, see Figure 6a. However, what is different is that the isotropic polarizability of all these complexes increases linearly with increasing cluster size, as shown in Figure 6b, similar to the Li₂-doped boron nitride clusters ($n = 4-8$) [8]. In particular, the doping of the K atom can be predicted to improve the α_{iso} values by $\sim 7-41\%$, indicating that the alkali metal atoms provide the possibility for inducing the isotropic polarizability. Additionally, according to the hard soft acids bases (HSAB) principle [62], the species with small HOMO-LUMO gaps are less hard and more polarizable, and this reveals that the large polarizabilities of the studied species have close relations with their small energy gaps.

As shown in Figure 6c, the variation of the first hyperpolarizabilities (β_{tot}) is interesting and has become the focus of our attention. One can see that the β_{tot} values of all the complexes distinctly decrease up to the size of $n = 6$, and are slightly fluctuating for larger sizes, with the exception of local maximum peaks, e.g., $n = 7, 9,$ and 12 . Compared with the bare Ge_nAu clusters, it is found that the alkali metals can dramatically enhance β_{tot} , but there are strong dependencies on the cluster size,

and they are more sensitive to the geometric structures. As shown in Figure 6c, the ordering of the enhanced β_{tot} values by alkali metals is nearly $\text{K} > \text{Na} > \text{Li}$, with exception of the $\text{Na@Ge}_7\text{Au}$ and $\text{Na@Ge}_{12}\text{Au}$ clusters. Clearly, the first hyperpolarizabilities of $\text{AM@Ge}_n\text{Au}$ ($\text{AM} = \text{Na}$ and K) are large enough to establish their strong nonlinear optical response, due to increased β_{tot} values ($\sim 140\text{--}6111\%$) induced by the two alkali metal atoms. Especially, the $\text{Na@Ge}_n\text{Au}$ ($n = 7$ and 12) and $\text{K@Ge}_n\text{Au}$ ($n = 2$ and 3) clusters possess remarkable NLO responses, with the β_{tot} values of 13,050, 6288, 9602, and 8812 a.u., respectively. Furthermore, the largest β_{tot} value (13,050 a.u.) of $\text{Na@Ge}_7\text{Au}$ is comparable to those of Li_2F (12,347 a.u.) [7] and $\text{Li}_2\text{@BN-clusters}(8,0)$ (12,282 a.u.) [8]. On the other hand, the largest β_{tot} values is also about 1.87 times larger than that of the $\text{Na@Si}_9\text{Nb}^+$ cluster (6987 a.u.), which has the largest β_{tot} value among the $\text{AM@Si}_n\text{Nb}^+$ clusters reported previously [16], and it shows that the germanium-based clusters doped by alkali metals provide the greater β_{tot} than the silicon-based clusters. This result suggests that the germanium-based clusters with the large β_{tot} , served as building blocks with tunable properties, may be promising for the design of novel macroscopic NLO materials.

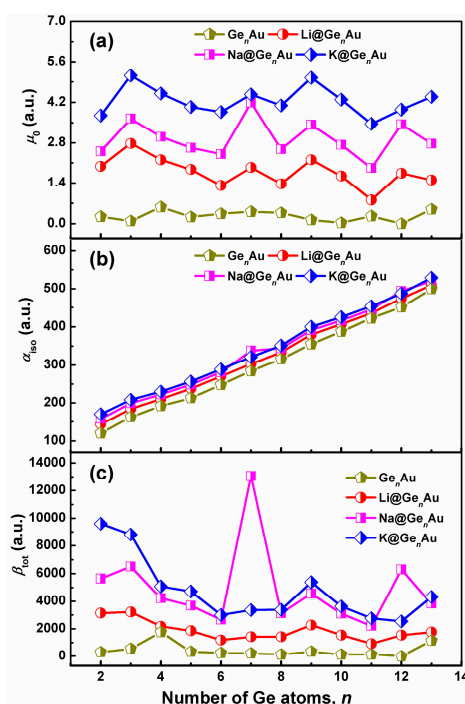


Figure 6. Comparison of evaluated (a) dipole moments (μ_0), (b) isotropic polarizabilities (α_{iso}), and (c) static first hyperpolarizability (β_{tot}) of $\text{AM@Ge}_n\text{Au}$ ($\text{AM} = \text{Li}, \text{Na},$ and $\text{K}; n = 2\text{--}13$) with Ge_nAu cluster, calculated at the CAM-B3LYP/def2-TZVPD level of theory.

To further understand the NLO behavior, we have performed the TDDFT calculations on the clusters with large β_{tot} values at the CAM-B3LYP/def2-TZVPD level of theory. The most widely common two-level model is considered and it gains more insight into the NLO response [40,63]. The static first hyperpolarizability can be expressed by the following equation:

$$\beta_{\text{tot}} \propto \frac{\Delta\mu \cdot f_0}{\Delta E^3} \quad (7)$$

where ΔE , f_0 , and $\Delta\mu$ are the transition energy, the oscillator strength, and the difference in dipole moment between the ground state and the crucial excited state, respectively. Of which the crucial excited state is specified by the largest f_0 value, and the third-power of transition energy is inversely proportional to the β_{tot} value. The calculated ΔE , f_0 , and $\Delta\mu$ values by TDDFT for the crucial excited states are listed in Table 1. One can see that the ΔE values for $\text{K@Ge}_2\text{Au}$, $\text{K@Ge}_3\text{Au}$, and $\text{Na@Ge}_7\text{Au}$

are 6.056 eV, 5.702 eV and 3.798 eV, respectively. The smallest ΔE corresponds to the first excited state of the Na@Ge₇Au cluster, which is in accordance with its largest β_{tot} value. Thus, the two-level approximation can be used for qualitative description of the polarization mechanism, and the low transition energy is the most significant factor in designing the nonlinear optical materials.

Table 1. The isotropic polarizabilities (α_{iso} , in a.u.), static first hyperpolarizability (β_{tot} , in a.u.), transition energy (ΔE , in eV), maximum oscillator strength (f_0 , in a.u.), and the change in dipole moment ($\Delta\mu$, in Debye) for crucial excited states of the following clusters.

Clusters	α_{iso}	β_{tot}	ΔE	f_0	$\Delta\mu$	Crucial Transitions * (%)
K@Ge ₂ Au	170	9602	6.056	0.358	0.371	H-3 → L+2 (42%)
K@Ge ₃ Au	209	8812	5.702	0.297	0.623	H → L+12 (18%), H-5 → L+2 (12%)
Na@Ge ₇ Au	338	13050	3.798	0.128	3.245	H-7 → L (28%), H-6 → L (17%), H-2 → L+4 (14%)

* H = HOMO, L = LUMO.

In order to explore the origin of the second-order NLO response, the molecular orbitals (MOs) features involving in the crucial transitions are presented in Figure 7. One can note that the crucial excitation of K@Ge₂Au originates from a HOMO-3 → LUMO+2 (42%) transition at ~205 nm, and the two MOs are mainly localized on the two Ge atoms with *s*-lone pairs, and the Au atom with the *d_{xy}*- and *p_y*-lone pairs, respectively. For K@Ge₃Au, however, the large absorption band at ~217 nm with $f_0 = 0.297$ ascribes to two mainly electron transitions, listed in Table 1, being the HOMO → LUMO+12 (18%) and HOMO-5 → LUMO+2 (12%) transitions, respectively. Of which the HOMO is mostly delocalized on the clusters surface (rhombic moiety) via the σ chemical bonds (e.g., Ge-Ge, Au-Ge, etc.), whereas the LUMO+12 is intensely localized on the K atom with the *p_x*-lone pair (see Figure 7). It is noteworthy that the strong transitions can be designated as intramolecular charge transfer, and this should be related to the large β_{tot} value. Moreover, the difference of charge transfer can give rise to various electronic effects, but all of other MOs contribute little to electronic transitions of the cluster ($\leq 8\%$). Table 1 lists the major contributions of electronic transition of the Na@Ge₇Au cluster in crucial excited states. Its strongest transitions can be assigned to be composed by three mainly mixed excitations of HOMO-7 → LUMO (28%), HOMO-6 → LUMO (17%), and HOMO-2 → LUMO+4 (14%). From Figure 7, it is evident that HOMO-7 is delocalized on QP's surface via σ bonds, and HOMO-2 and HOMO-6 can be formed by two π bonds, located at the inner and outer QP, whereas the electron distributions of LUMO are mainly associated with the Na-Au bond instead of other atoms, and LUMO+4 is mostly delocalized on the QP's surface with additional distribution on Au atom. Therefore, the situation of intramolecular charge transfer of cluster directly influences the transition energy, which is a decisive factor that leads to a considerably large first hyperpolarizability.

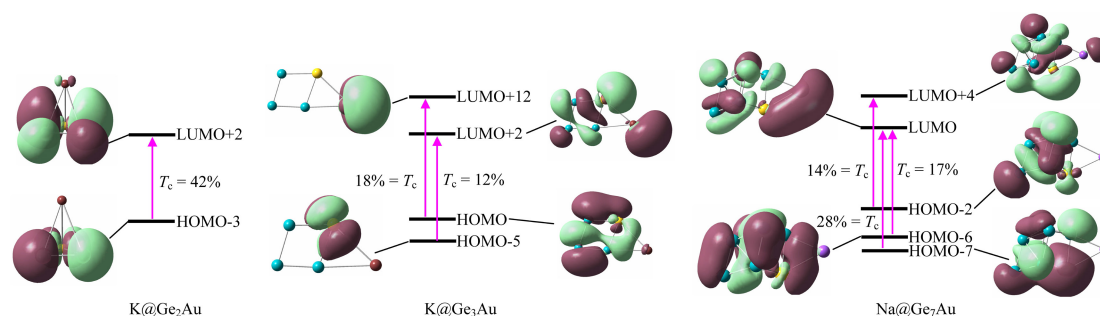


Figure 7. Frontier molecular orbitals involving in the crucial transitions (T_c) for the K@Ge₂Au, K@Ge₃Au, and Na@Ge₇Au clusters, computed at the CAM-B3LYP/def2-TZVPD level of theory.

4. Conclusions

In the present work, we have systematically investigated the structures, chemical stabilities and nonlinear optical properties as well as the chemical bonding and electronic structures of a series of alkali metals-adsorbed gold-germanium bimetallic clusters using the hybrid DFT-B3LYP method. Structurally, it has been determined that the adsorption of alkali metal atoms does not largely affect the structural framework of the gold-germanium clusters, and the alkali metals prefer energetically to be attached on clusters' surface or edge. The Li-adsorbed bicapped pentagonal prism of the Li@Ge₁₂Au cluster is electronically stable due to obeying the spherical aromaticity counting rule. Meanwhile, the molecular orbitals analysis reveals that the Au-4*d* state has strong interactions with the germanium atoms, and the hybridization between the Ge and Au atoms can enhance the chemical stability of the bimetallic cluster. This AdNDP analysis indicates that the localized 2c-2e σ -bonds are located on the clusters' surface, while all the delocalized σ -bonds are involved in the endohedral Au dopant, which are responsible for structural stabilization of Li@Ge₁₂Au. The static first hyperpolarizabilities are strongly related to the cluster size and geometric structure, and the AM@Ge_{*n*}Au (AM = Na and K) clusters display the large β_{tot} values, which are enough to establish their strong nonlinear optical behaviors, especially for Na@Ge_{*n*}Au (*n* = 7 and 12) and K@Ge_{*n*}Au (*n* = 2 and 3). The present results will inevitably stimulate future experimental and theoretical studies of germanium-based semiconductor clusters doped by alkali metals for the design of novel nonlinear optical materials.

Supplementary Materials: The following are available online at <http://www.mdpi.com/2079-4991/7/7/184/s1>. Table S1: Comparison of relative energies for the low-lying neutral AM@Ge_{*n*}Au (AM = Li, Na, and K; *n* = 2–13) clusters, calculated by using the hybrid DFT-B3LYP functionals together with two different basis sets.

Acknowledgments: This work was supported by the National Natural Science Foundation of China (Nos. 21603173, 21643014, and 21303135), the Natural Science Foundation of Shaanxi Province (Nos. 2016JQ5110, 2016JQ2030), the Special Natural Science Foundation of Science and Technology Bureau of Xi'an City (Nos. 2016CXWL16, 2016CXWL02, and 2016CXWL18).

Author Contributions: Xiaojun Li conceived and designed the project, performed the chemical bonding analyses and the linear and nonlinear optical (L&NLO) properties with all of the members, and wrote the manuscript; Shuna Li carried out the structural optimizations and contributed to the density of states; Hongjiang Ren analyzed the chemical stabilities of clusters and electronic structures; Juxiang Yang performed the TDDFT calculations and analyzed the results; Yongqiang Tang analyzed the spherical aromaticity. All authors contributed to the interpretation and discussion of the data at all stages.

Conflicts of Interest: The authors declare no conflict of interest.

References

1. Khanna, S.N.; Jena, P. Atomic clusters: Building blocks for a class of solids. *Phys. Rev. B* **1995**, *51*, 13705. [[CrossRef](#)]
2. Hou, N.; Wu, D.; Li, Y.; Li, Z.-R. Lower the electron affinity by halogenation: An unusual strategy to design superalkali cations. *J. Am. Chem. Soc.* **2014**, *136*, 2921–2927. [[CrossRef](#)] [[PubMed](#)]
3. Zhang, C.-C.; Xu, H.-L.; Hu, Y.-Y.; Sun, S.-L.; Su, Z.-M. Quantum chemical research on structures, linear and nonlinear optical properties of the Li@*n*-acenes salt (*n* = 1, 2, 3, and 4). *J. Phys. Chem. A* **2011**, *115*, 2035–2040. [[CrossRef](#)] [[PubMed](#)]
4. Sun, W.-M.; Wu, D.; Li, Y.; Li, Z.-R. Theoretical study on superalkali (Li₃) in ammonia: Novel alkalides with considerably large first hyperpolarizabilities. *Dalton Trans.* **2014**, *43*, 486–494. [[CrossRef](#)] [[PubMed](#)]
5. Yaghobi, M.; Rafie, R.; Koochi, A. Optical and structural properties of the endohedral complexes M@C₆₀ (M = Cs, Li, and Na). *J. Mol. Struct. THEOCHEM* **2009**, *905*, 48–50. [[CrossRef](#)]
6. Wang, S.-J.; Li, Y.; Wang, Y.-F.; Wu, D.; Li, Z.-R. Structures and nonlinear optical properties of the endohedral metallofullerene-superhalogen compounds Li@C₆₀-BX₄ (X = F, Cl, Br). *Phys. Chem. Chem. Phys.* **2013**, *15*, 12903–12910. [[CrossRef](#)] [[PubMed](#)]
7. Srivastava, A.K.; Misra, N. Nonlinear optical behavior of Li_{*n*}F (*n* = 2–5) superalkali clusters. *J. Mol. Model.* **2015**, *21*, 305. [[CrossRef](#)] [[PubMed](#)]

8. Ma, F.; Zhou, Z.-J.; Liu, Y.-T. Li_2 trapped inside tubiform $[n]$ boron nitride clusters ($n = 4-8$): Structures and first hyperpolarizability. *ChemPhysChem* **2012**, *13*, 1307–1312. [[CrossRef](#)] [[PubMed](#)]
9. Srivastava, A.K.; Misra, N. Competition between alkalide characteristics and nonlinear optical properties in $\text{OLi}_3\text{-M-Li}_3\text{O}$ ($\text{M} = \text{Li, Na, and K}$) complexes. *Int. J. Quantum Chem.* **2017**, *117*, 208–212. [[CrossRef](#)]
10. Sun, W.-M.; Fan, L.-T.; Li, Y.; Liu, J.-Y.; Wu, D.; Li, Z.-R. On the potential application of superalkali clusters in designing novel alkalides with large nonlinear optical properties. *Inorg. Chem.* **2014**, *53*, 6170–6178. [[CrossRef](#)] [[PubMed](#)]
11. Jing, Y.-Q.; Li, Z.-R.; Wu, D.; Li, Y.; Wang, B.-Q.; Gu, F.L.; Aoki, Y. Effect of the complexant shape on the large first hyperpolarizability of alkalides $\text{Li}^+(\text{NH}_3)_4\text{M}^-$. *ChemPhysChem* **2006**, *7*, 1759–1763. [[CrossRef](#)] [[PubMed](#)]
12. DeBacker, M.G.; Mkadmi, E.B.; Sauvage, F.X.; Lelieur, J.-P.; Wagner, M.J.; Concepcion, R.; Kim, J.; McMills, L.E.H.; Dye, J.L. The lithium-sodium-methylamine system: Does a low-melting sodide become a liquid metal? *J. Am. Chem. Soc.* **1996**, *118*, 1997–2003. [[CrossRef](#)]
13. Muhammad, S.; Xu, H.; Liao, Y.; Kan, Y.; Su, Z. Quantum mechanical design and structure of the $\text{Li}@\text{B}_{10}\text{H}_{14}$ basket with a remarkably enhanced electro-optical response. *J. Am. Chem. Soc.* **2009**, *131*, 11833–11840. [[CrossRef](#)] [[PubMed](#)]
14. Xu, H.-L.; Li, Z.-R.; Su, Z.-M.; Muhammad, S.; Gu, F.L.; Harigaya, K. Knot-isomers of möbius cyclacene: How does the number of knots influence the structure and first hyperpolarizability? *J. Phys. Chem. C* **2009**, *113*, 15380–15383. [[CrossRef](#)]
15. Karamanis, P.; Marchal, R.; Carbonnière, P.; Pouchan, C. Doping-enhanced hyperpolarizabilities of silicon clusters: A global ab initio and density functional theory study of Si_{10} (Li, Na, K) $_n$ ($n = 1, 2$) clusters. *J. Chem. Phys.* **2011**, *135*, 044511. [[CrossRef](#)] [[PubMed](#)]
16. Li, X.; Han, Q.; Yang, X.; Song, R.; Song, L. Modification of alkali metals on silicon-based nanoclusters: An enhanced nonlinear optical response. *Chem. Phys. Lett.* **2016**, *659*, 93–99. [[CrossRef](#)]
17. Donoso-Tauda, O.; Yepes, D.; Jaque, P.; Santos, J.C. Stability analysis of lithio-silicon $\text{Si}_{10}\text{Li}_8$ clusters: Planar bicyclic ring vs. Three-dimensional structures. *Chem. Phys. Lett.* **2014**, *604*, 72–76. [[CrossRef](#)]
18. Li, X.; Su, K.; Yang, X.; Song, L.; Yang, L. Size-selective effects of geometry and electronic property on bimetallic au-ge nanoclusters. *Comput. Theor. Chem.* **2013**, *1010*, 32–37. [[CrossRef](#)]
19. Deng, X.-J.; Kong, X.-Y.; Xu, X.-L.; Xu, H.-G.; Zheng, W.-J. Structural and magnetic properties of CoGe_n^- ($n = 2-11$) clusters: Photoelectron spectroscopy and density functional calculations. *ChemPhysChem* **2014**, *15*, 3987–3993. [[CrossRef](#)] [[PubMed](#)]
20. Li, X.; Claes, P.; Haertelt, M.; Lievens, P.; Janssens, E.; Fielicke, A. Structural determination of niobium-doped silicon clusters by far-infrared spectroscopy and theory. *Phys. Chem. Chem. Phys.* **2016**, *18*, 6291–6300. [[CrossRef](#)] [[PubMed](#)]
21. Ngan, V.T.; Haeck, J.D.; Le, H.T.; Gopakumar, G.; Lievens, P.; Nguyen, M.T. Experimental detection and theoretical characterization of germanium-doped lithium clusters Li_nGe ($n = 1-7$). *J. Phys. Chem. A* **2009**, *113*, 9080–9091. [[CrossRef](#)] [[PubMed](#)]
22. Li, X.; Yan, Z.; Li, S. The nature of structure and bonding between transition metal and mixed si-ge tetramers: A 20-electron superatom system. *J. Comput. Chem.* **2016**, *37*, 2316–2323. [[CrossRef](#)] [[PubMed](#)]
23. Lu, S.-J.; Xu, X.-L.; Feng, G.; Xu, H.-G.; Zheng, W.-J. Structural and electronic properties of AuSi_n^- ($n = 4-12$) clusters: Photoelectron spectroscopy and ab initio calculations. *J. Phys. Chem. C* **2016**, *120*, 25628–25637. [[CrossRef](#)]
24. Li, X.; Su, K. Structure, stability and electronic property of the gold-doped germanium clusters: AuGe_n ($n = 2-13$). *Theor. Chem. Acc.* **2009**, *124*, 345–354. [[CrossRef](#)]
25. Li, X.; Li, C.; Yang, J.; Jalbout, A.F. The structures, thermochemistry, and electron affinities of hydrogenated silicon clusters $\text{Si}_6\text{H}_n/\text{Si}_6\text{H}_n^-$ ($n = 3-14$). *Int. J. Quantum Chem.* **2009**, *109*, 1283–1301. [[CrossRef](#)]
26. Xenides, D.; Karamanis, P.; Pouchan, C. A critical analysis of the performance of new generation functionals on the calculation of the (hyper) polarizabilities of clusters of varying stoichiometry: Test case the Si_mGe_n ($m + n = 7, n = 0-7$) clusters. *Chem. Phys. Lett.* **2010**, *498*, 134–139. [[CrossRef](#)]
27. Knoppe, S.; Hakkinen, H.; Verbiest, T. Nonlinear optical properties of thiolate-protected gold clusters: A theoretical survey of the first hyperpolarizabilities. *J. Phys. Chem. C* **2015**, *119*, 27676–27682. [[CrossRef](#)]
28. Knoppe, S.; Vanbel, M.; van Cleuvenbergen, S.; Vanpraet, L.; Buergi, T.; Verbiest, T. Nonlinear optical properties of thiolate-protected gold clusters. *J. Phys. Chem. C* **2015**, *119*, 6221–6226. [[CrossRef](#)]

29. Ozga, K.; Kawaharamura, T.; Umar, A.A.; Oyama, M.; Nouneh, K.; Slezak, A.; Fujita, S.; Piasecki, M.; Reshak, A.H.; Kityk, I.V. Second order optical effects in Au nanoparticle-deposited ZnO nanocrystallite films. *Nanotechnology* **2008**, *19*, 185709. [[CrossRef](#)] [[PubMed](#)]
30. Becke, A.D. Density-functional exchange-energy approximation with correct asymptotic behavior. *Phys. Rev. A* **1988**, *38*, 3098–3100. [[CrossRef](#)]
31. Lee, C.; Yang, W.; Parr, R.G. Development of the colle-salvetti correlation-energy formula into a functional of the electron density. *Phys. Rev. B* **1988**, *37*, 785–789. [[CrossRef](#)]
32. Frisch, M.J.; Trucks, G.W.; Schlegel, H.B.; Scuseria, G.E.; Robb, M.A.; Cheeseman, J.R.; Scalmani, G.; Barone, V.; Mennucci, B.; Petersson, G.A.; et al. *Gaussian 09, Revision D. 01*; Gaussian, Inc.: Wallingford, CT, USA, 2009.
33. Ngan, V.T.; Nguyen, M.T. The aromatic 8-electron cubic silicon clusters Be@Si_8 , B@Si_8^+ , and C@Si_8^{2+} . *J. Phys. Chem. A* **2010**, *114*, 7609–7615. [[CrossRef](#)] [[PubMed](#)]
34. Bauschlicher, C.W. A comparison of the accuracy of different functionals. *Chem. Phys. Lett.* **1995**, *246*, 40–44. [[CrossRef](#)]
35. Garoufalidis, C.S.; Zdetsis, A.D.; Grimme, S. High level ab initio calculations of the optical gap of small silicon quantum dots. *Phys. Rev. Lett.* **2001**, *87*, 276402. [[CrossRef](#)] [[PubMed](#)]
36. Hay, P.J.; Wadt, W.R. Ab initio effective core potentials for molecular calculations. Potentials for the transition metal atoms Sc to Hg. *J. Chem. Phys.* **1985**, *82*, 270–283. [[CrossRef](#)]
37. Wadt, W.R.; Hay, P.J. Ab initio effective core potentials for molecular calculations. Potentials for main group elements Na to Bi. *J. Chem. Phys.* **1985**, *82*, 284–298. [[CrossRef](#)]
38. Hay, P.J.; Wadt, W.R. Ab initio effective core potentials for molecular calculations. Potentials for K to Au including the outermost core orbitals. *J. Chem. Phys.* **1985**, *82*, 299–310. [[CrossRef](#)]
39. Lu, S.-J.; Hu, L.-R.; Xu, X.-L.; Xu, H.-G.; Chen, H.; Zheng, W.-J. Transition from exohedral to endohedral structures of AuGe_n^- ($n = 2\text{--}12$) clusters: Photoelectron spectroscopy and ab initio calculations. *Phys. Chem. Chem. Phys.* **2016**, *18*, 20321–20329. [[CrossRef](#)] [[PubMed](#)]
40. Kanis, D.R.; Ratner, M.A.; Marks, T.J. Design and construction of molecular assemblies with large second-order optical nonlinearities. Quantum chemical aspects. *Chem. Rev.* **1994**, *94*, 195–242. [[CrossRef](#)]
41. Li, X.; Ren, H.; Yang, X.; Song, J. Exploring the chemical bonding, infrared and UV–vis absorption spectra of oh radicals adsorption on the smallest fullerene. *Spectrochim. Acta Part A* **2015**, *144*, 258–265. [[CrossRef](#)] [[PubMed](#)]
42. Cohen, H.D.; Roothaan, C.C.J. Electric dipole polarizability of atoms by the hartree-fock method. I. Theory for closed-shell systems. *J. Chem. Phys.* **1965**, *43*, S34–S39. [[CrossRef](#)]
43. O’Boyle, N.M.; Tenderholt, A.L.; Langner, K.M. Cclib: A library for packageindependent computational chemistry algorithms. *J. Comp. Chem.* **2008**, *29*, 839–845. [[CrossRef](#)] [[PubMed](#)]
44. Zubarev, D.Y.; Boldyrev, A.I. Developing paradigms of chemical bonding: Adaptive natural density partitioning. *Phys. Chem. Chem. Phys.* **2008**, *10*, 5207–5217. [[CrossRef](#)] [[PubMed](#)]
45. Humphrey, W.; Dalke, A.; Schulten, K. Vmd: Visual molecular dynamics. *J. Mol. Graph.* **1996**, *14*, 33–38. [[CrossRef](#)]
46. Yanaia, T.; Tew, D.P.; Handy, N.C. A new hybrid exchange—Correlation functional using the coulomb-attenuating method (CAM-B3LYP). *Chem. Phys. Lett.* **2004**, *393*, 51–57. [[CrossRef](#)]
47. Li, X.; Hopmann, K.H.; Hudecová, J.; Isaksson, J.; Novotná, J.; Stensen, W.; Andrushchenko, V.; Urbanová, M.; Svendsen, J.-S.; Bouř, P.; et al. Determination of absolute configuration and conformation of a cyclic dipeptide by nmr and chiral spectroscopic methods. *J. Phys. Chem. A* **2013**, *117*, 1721–1736. [[CrossRef](#)] [[PubMed](#)]
48. Kumar, V.; Kawazoe, Y. Metal-encapsulated icosahedral superatoms of germanium and tin with large gaps: Zn@Ge_{12} and Cd@Sn_{12} . *Appl. Phys. Lett.* **2002**, *80*, 859–861. [[CrossRef](#)]
49. Mahtout, S.; Tariket, Y. Electronic and magnetic properties of CrGe_n ($15 \leq n \leq 29$) clusters: A DFT study. *Chem. Phys.* **2016**, *472*, 270–277. [[CrossRef](#)]
50. Tai, T.B.; Nguyen, M.T. A stochastic search for the structures of small germanium clusters and their anions: Enhanced stability by spherical aromaticity of the Ge_{10} and Ge_{12}^{2-} systems. *J. Chem. Theory Comput.* **2011**, *7*, 1119–1130. [[CrossRef](#)] [[PubMed](#)]
51. Brack, M. The physics of simple metal clusters: Self-consistent jellium model and semiclassical approaches. *Rev. Mod. Phys.* **1993**, *65*, 677–732. [[CrossRef](#)]
52. Zhai, H.-J.; Zhao, Y.-F.; Li, W.-L.; Chen, Q.; Bai, H.; Hu, H.-S.; Piazza, Z.A.; Tian, W.-J.; Lu, H.-G.; Wu, Y.-B.; et al. Observation of an all-boron fullerene. *Nat. Chem.* **2014**, *6*, 727–731. [[CrossRef](#)] [[PubMed](#)]

53. Popov, I.A.; Li, W.-L.; Piazza, Z.A.; Boldyrev, A.I.; Wang, L.-S. Complexes between planar boron clusters and transition metals: A photoelectron spectroscopy and ab initio study of CoB_{12}^- and RhB_{12}^- . *J. Phys. Chem. A* **2014**, *118*, 8098–8105. [[CrossRef](#)] [[PubMed](#)]
54. Boldyrev, A.; Wang, L.-S. Beyond organic chemistry: Aromaticity in atomic clusters. *Phys. Chem. Chem. Phys.* **2016**, *18*, 11589–11605. [[CrossRef](#)] [[PubMed](#)]
55. Popov, I.A.; Jian, T.; Lopez, G.V.; Boldyrev, A.I.; Wang, L.-S. Cobalt-centred boron molecular drums with the highest coordination number in the cob_{16}^- cluster. *Nat. Commun.* **2015**, *6*, 8654. [[CrossRef](#)] [[PubMed](#)]
56. Boldyrev, A.I.; Wang, L.-S. All-metal aromaticity and antiaromaticity. *Chem. Rev.* **2005**, *105*, 3716–3757. [[CrossRef](#)] [[PubMed](#)]
57. Hirsch, A.; Chen, Z.; Jiao, H. Spherical aromaticity in i_h symmetrical fullerenes: The $2(n + 1)^2$ rule. *Angew. Chem. Int. Ed.* **2000**, *39*, 3915–3917. [[CrossRef](#)]
58. Hirsch, A.; Chen, Z.; Jiao, H. Spherical aromaticity of inorganic cage molecules. *Angew. Chem. Int. Ed.* **2001**, *40*, 2834–2838. [[CrossRef](#)]
59. Tai, T.B.; Nguyen, M.T. Lithium atom can be doped at the center of a germanium cage: The stable icosahedral $\text{ge}_{12}\text{li}^-$ cluster and derivatives. *Chem. Phys. Lett.* **2010**, *492*, 290–296. [[CrossRef](#)]
60. King, R.B.; Heine, T.; Corminboeuf, C.; Schleyer, P.v.R. Antiaromaticity in bare deltahedral silicon clusters satisfying wade's and hirsch's rules: An apparent correlation of antiaromaticity with high symmetry. *J. Am. Chem. Soc.* **2004**, *126*, 430–431. [[CrossRef](#)] [[PubMed](#)]
61. Chen, Z.; Wannere, C.S.; Corminboeuf, C.; Puchta, R.; Schleyer, P.v.R. Nucleus-independent chemical shifts (NICS) as an aromaticity criterion. *Chem. Rev.* **2005**, *105*, 3842–3888. [[CrossRef](#)] [[PubMed](#)]
62. Pearson, R.G. Hard and soft acids and bases. *J. Am. Chem. Soc.* **1963**, *85*, 3533–3539. [[CrossRef](#)]
63. Oudar, J.L. Optical nonlinearities of conjugated molecules. Stilbene derivatives and highly polar aromatic compounds. *J. Chem. Phys.* **1977**, *67*, 446–457. [[CrossRef](#)]



© 2017 by the authors. Licensee MDPI, Basel, Switzerland. This article is an open access article distributed under the terms and conditions of the Creative Commons Attribution (CC BY) license (<http://creativecommons.org/licenses/by/4.0/>).